Real-time integration of cell death and proliferation kinetics at the single-cell and population-level using high-throughput live-cell imaging

Jesse D. Gelles[1,2,3], Jarvier N. Mohammed[1,2,3], Luis C. Santos[1], and Jerry E. Chipuk[1,2,3,4,5,*]

[1] Department of Oncological Sciences,

[2] The Tisch Cancer Institute,

[3] The Graduate School of Biomedical Sciences,

[4] Department of Dermatology,

[5] The Diabetes, Obesity, and Metabolism Institute,

Icahn School of Medicine at Mount Sinai, One Gustave L. Levy Place, Box 1130, New York, New York 10029 USA

*Corresponding author: jerry.chipuk@mssm.edu

Summary

Quantifying cytostatic and cytotoxic outcomes are integral components of characterizing perturbagens used as research tools and/or in drug discovery pipelines. Furthermore, data-rich acquisition coupled with robust methods for analysis is required to properly assess the function and impact of these perturbagens. Here, we present a detailed and versatile method for Single-cell and Population-level Analyses using Real-time Kinetic Labeling (SPARKL). SPARKL integrates high-content live-cell imaging with automated detection and analysis of fluorescent reporters of cell death. We outline several examples of zero-handling, non-disruptive protocols for detailing cell death mechanisms and proliferation profiles. Additionally, we suggest several methods for mathematically analyzing these data to best utilize the collected kinetic data. Compared to traditional methods of detection and analysis, SPARKL is highly sensitive, accurate, and extremely high-throughput while substantially eliminating sample processing and providing richer data.

Keywords

Apoptosis, Automated image analysis, Cell Death, High-throughput, Live-cell imaging, Real-time assay

Acknowledgements

This work was supported by: NIH grants CA157740 (J.E.C.), CA206005 (J.E.C.), and F31AA024681 (J.D.G.), the JJR Foundation, the William A. Spivak Fund, the Fridolin Charitable Trust, an American Cancer Society Research Scholar Award, a Leukemia & Lymphoma Society Career Development Award, and an Irma T. Hirschl/Monique Weill-Caulier Trust Research Award. This work was also supported in part by two research grants (5FY1174 and 1FY13416) from the March of Dimes Foundation, and the Developmental Research Pilot Project Program within the Department of Oncological Sciences at the Icahn School of Medicine at Mount Sinai, and the Tisch Cancer Institute Cancer Center Support Grant (P30 CA196521).

Conflict of Interest

The authors declare no conflict of interest.

Abbreviations

BAX: BCL-2-associated X protein; BAK: BCL-2 homologous antagonist killer; BCL-2: B-cell lymphoma 2; BCL-xL: B-cell lymphoma-extra large; CFSE: Carboxyfluorescein succinimidyl ester; CHX: cycloheximide; DMEM: Dulbecco's modified Eagle's medium; FBS: fetal bovine serum; FITC: Fluorescein isothiocyanate; MEF: mouse embryonic fibroblast; NHS Esters: N-hydroxysuccinimide esters; PARP: poly ADP ribose polymerase; PBS: phosphate-buffered saline; PI: propidium iodide; PS: phosphatidylserine; ROI: Region of interest; STS: staurosporine; TNFα: tumor necrosis

factor α; TRAIL: TNF-related apoptosis-inducing ligand; UPR: unfolded protein response; zVAD-fmk: carbobenzoxy-valyl-alanyl-aspartyl-[O-methyl]-fluoromethylketone.

Author Contributions

Conceptualization: J.D.G.; Funding Acquisition: J.D.G. and J.E.C.; Investigation: J.D.G. and J.N.M.; Methodology: J.D.G.; Project Administration: J.D.G.; Software: L.C.S.; Supervision: J.E.C.; Validation: J.N.M., Visualization: J.D.G.; Writing: J.D.G., J.N.M., and J.E.C.

Introduction

Programmed cell death pathways are conserved signaling mechanisms which developed early in the evolution of metazoa. One aspect shared between many programmed cell death pathways is a variable lag phase between the exposure to a perturbagen and the cell's commitment to a cell death program. This lag phase is the consequence of intersecting intracellular pro-death and pro-survival signal transduction and provides the cell with an opportunity to resolve the stress signal and repair accumulated damage (Biton and Ashkenazi, 2011). If these insults are not resolved, the pro-death signaling contributions will overwhelm the antagonistic pro-survival pathway and trigger biological events committing the cell to death. Importantly, in apoptosis this lag phase also contains an orchestrated and systematic dissolution of organelles and cellular components conducive to efficient clearance with minimal perturbation to neighboring cells. This process is exemplified in apoptosis by the BCL-2 family of proteins, consisting of pro-apoptotic effector proteins (e.g., BAX, BAK) and anti-apoptotic proteins (e.g., BCL-2, BCL-xL), which ultimately serve to regulate the permeabilization of the outer mitochondrial membrane and subsequent activation of the caspase cascade (Wei et al., 2001, Chipuk et al., 2010). However, the kinetics and perpetuation of cell death signaling is highly variable between perturbagens, cell types, death pathways, and between sister cells within a population (Spencer et al., 2009; Gaudet et al., 2012). Elucidating the underlying biology which causes this variability remains a principle focus within the fields of cell death, cell biology, and drug discovery (Kepp et al., 2011). To this end, development of technologies to properly observe and analyze cell death is crucial to the progression of these fields of study.

Current standard methods used to observe and quantify cell death remain outdated, suffer from limited throughput, and generate limited datasets for interpretation. The detection and quantification of dead or dying cells is most commonly accomplished by flow cytometry, which requires non-trivial cell numbers, extensive sample handling, sample exposure to significant mechanical and chemical stress, and creates considerable delays between sample harvesting and analyses (Koopman et al., 1994). For example, experiments must be terminated in order to be assayed and therefore only provide static endpoint data, requiring considerable effort to optimize the experimental design.

Commonly used reagents involve cell-impermeable “viability” dyes (such as propidium iodide, DRAQ7, SYTOX, and YOYO3), which label cells following loss of plasma membrane integrity and permeabilization. Reliance on this feature for quantification does not distinguish between distinct pathways and labels cells at the tail-end of the dismantling process, thereby failing to capture the time in which cells undergo key biological processes (Vanden Berghe et al., 2010; Dillon et al., 2014). Additionally, labeling by viability dyes is not stoichiometric and often results in pseudo-binary labeling profiles following the first instance of membrane instability. Enzymatically-cleaved fluorescently-conjugated probes (e.g., DEVD-containing caspase-target peptides) are another common strategy despite their cost, difficulty of use, poor signal, and differential and non-specific activation (Yu et al., 2001). Alternative methodologies use metabolic activity or biochemical measures as surrogate readouts for cell viability, but interpretations from this data are obfuscated by the underlying biology of the perturbagens and ultimately do not directly rely on cell death machinery (Chan et al., 2013).

Design

Here, we integrate and expand upon multiple previously described methods for observing and quantifying cell proliferation and cell death using live-cell high-content imagers and refer to this method as Single-cell and Population-level Analyses using Real-time Kinetic Labeling (SPARKL). We utilize fluorescently-labeled Annexin V due to its stability, signal strength and longevity, stoichiometric binding, and relevance to cell death machinery. Our non-toxic label-and-go methods outperform previous methodologies while maintaining high-sensitivity, high-accuracy, and a high-throughput zero-handling rapid protocol. Furthermore, we expand on the versatility of our method by providing several example adaptations and mathematical analyses to explore the depth of the collected kinetic data. Collectively, these examples demonstrate how data gathered using SPARKL can be used to investigate fundamental aspects of cell death biology.

Results and Discussion

Automated live-cell imaging and detection of fluorescent labeling provides rich datasets for analyzing cell death in response to perturbagens.

We developed SPARKL chiefly to capture kinetic cell death data since traditional methods utilizing flow cytometry are limited to endpoint data. Additionally, we aimed to design a workflow compatible with high-throughput studies while requiring minimal handling and retaining high sensitivity and specificity. Here, we capitalize on the advent of high-content in-incubator live-cell imagers to capture cellular phenotypes, measure fluorescent signals, and analyze data in real-time through regular scanning schedules. This technology eliminates the requirement for disruptive handling and is non-invasive to cells in culture. The repeated observation of samples and coupled automated real-time analysis also collects richer datasets in a workflow that is less labor- and time-intensive than analogous workflows using flow cytometry (Figure 1A).

One benefit of this method is that cells are incubated in normal growth media containing fluorescent probes in order to eliminate stepwise processing to label samples. Therefore, detection reagents must be non-disruptive, highly specific, culture-stable, non-labile, and readily detectable when incubated with cells for prolonged period of time. Annexin V labels apoptotic cells by detecting phosphatidylserine (PS) on the outer leaflet of the plasma membrane, which is exposed during caspase-dependent cell death (Devaux, 1991). We began studies by testing FITC-labeled recombinant Annexin V and viability dye YOYO3 for compatibility within our method (Logue et al., 2009; Gelles and Chipuk, 2016). MEFs were cultured in growth media containing Annexin V and YOYO3, co-treated with tumor necrosis factor α (TNFα) and cycloheximide (CHX) to promote

apoptosis, and subjected to SPARKL using an in-incubator high-content live-cell imager. The kinetic data captured the lag phase followed by the robust labeling of MEFs undergoing death (Figure 1B). Here, cells were cultured in media containing sufficient calcium for robust Annexin V labeling, but alternative media formulations may require calcium supplementation (Meers and Mealy, 1993). Importantly, cells not treated with TNFα and CHX exhibited no toxicity as a consequence of either fluorescent probe (Figure 1B, “UT” line). As expected, the stoichiometric method of Annexin V-labeling was observed as the concentration-dependent decrease in number of positive events; by contrast, YOYO3-labeling exhibited binary labeling. To investigate if growth media containing colorimetric indicators might affect detection of fluorescent signals, we compared signal detection of MEFs instigated to die when incubated in DMEM lacking or containing phenol red. Events of cells labeled with either Annexin V-FITC or YOYO3 exhibited diminished average fluorescent intensity when culture media contained phenol red (Figure 1C). Therefore, all future applications of SPARKL utilized phenol red-free culture media.

The foundation of this method is the collection of high-content images of cells in culture at regular intervals which provide phenotypic characterization of cell populations, confluency data, and detection of fluorescent pixels. To demonstrate the diversity and specificity of data collected with SPARKL, *Bax*$^{+/+}$*Bak*$^{+/+}$ and *Bax*$^{-/-}$*Bak*$^{-/-}$ (WT and DKO, respectively) MEFs were cultured in media containing Annexin V-FITC and YOYO3, treated with perturbagens, and subjected to the SPARKL workflow. Images from select timepoints were manually reviewed to observe cellular morphology and detection of fluorescent labeling (Figure 1D). Green and red pixels from each collected image were

quantified using a trained algorithm and reported as the number of Annexin V- and YOYO3-positive events observed at each timepoint (Figure 1E). To assess the selectivity our fluorescent probes, MEFs were instigated to die through the extrinsic pathway of apoptosis (via co-treatment of TNFα+CHX), the intrinsic pathway of apoptosis (via topoisomerase inhibitor, VP16), or non-apoptotic pathway of ferroptosis (via cysteine-glutamate antiport inhibitor, erastin) (Peltzer et al., 2016; Dixon et al., 2012). Both Annexin V and YOYO3 demonstrated accuracy and selectivity by labeling cells in a time-dependent manner. Interestingly, VP16-treated MEFs exhibited the longest lag phase before onset of death and demonstrated Annexin V-positivity more rapidly than YOYO3-positivity, which reflects the biology of PS exposure prior to loss of plasma membrane asymmetry during apoptosis. To directly compare Annexin V-positivity between WT and DKO MEFs, data collected at specific timepoints were extracted and visualized side-by-side (Figure 1F). Data visualized in this manner highlights the differential labeling in cell treated with inducers of an apoptotic pathway. Of note, collection and visualization of these data from DKO MEFs treated with VP16 reveals that the morphological phenotypes observed in these cells does not coincide with probe labeling and therefore is not indicative of cell death (Figures 1D-F). This example exemplifies the benefits of collecting data using SPARKL for thorough interpretation of experimental results.

Investigations of apoptotic cell death commonly employ Annexin V-binding assays due to the exposure of PS on the outer leaflet of the plasma membrane following caspase-mediated cleavage of flippases (Segawa et al., 2014). Exposure of PS is indicative of the underlying apoptotic signaling, and precedes loss of plasma membrane integrity caused by breakdown of cellular homeostatic processes. Therefore, apoptotic studies

occasionally utilize a dual-labeling methodology of Annexin V with a viability dye in order to characterize cells in early- or late-apoptosis by dichotomizing single-positive and dual-positive events (Jiang et al., 2016). However, cells undergoing non-apoptotic cell death often do not exhibit this sequential labeling because loss of plasma membrane integrity occurs without the preceding exposure of PS and permits intracellularly labeling by Annexin V. As a consequence, cells label with the viability dye and Annexin V simultaneously, which is indistinguishable from cells in late-apoptosis when analyzed by flow cytometry (Figure 2A). Therefore, we investigated whether the kinetic data captured in SPARKL could be analyzed to distinguish between apoptotic and non-apoptotic cell death following treatment of cellular perturbagens.

In order to assess the capability of SPARKL to dichotomize kinetic labeling patterns of cells undergoing apoptotic or non-apoptotic cell death, we cultured WT MEFs in growth media containing Annexin V-FITC, YOYO3, and perturbagens engaging either the extrinsic pathway of apoptosis (TNFα+CHX), intrinsic pathway of apoptosis (CHX or VP16), or non-apoptotic ferroptosis (erastin) (Figure 2B). Cell populations instigated to die by TNFα+CHX co-treatment or VP16 exhibited Annexin V-positivity prior to YOYO3-positivity, indicative of apoptotic cell death. By contrast, cells instigated to die by high concentrations of CHX alone or erastin demonstrated similar kinetics of labeling with Annexin V and YOYO3. Additionally, we co-treated cells with ABT-737 (an inhibitor to multiple anti-apoptotic BCL-2 proteins) and zVAD-fmk (a pan-caspase inhibitor) to further characterize mechanisms of cell death in response to each perturbagen using the SPARKL assay (Oltersdorf et al., 2005; McStay et al., 2008). Cells dying via apoptosis demonstrated accelerated or attenuated rates of Annexin V-labeling in response to co-

treatment with ABT-737 or zVAD-fmk, respectively; cells dying via ferroptosis demonstrated no change in kinetics of Annexin V labeling. By comparison, kinetics of YOYO3 labeling exhibited less resolution and only modest changes in cells co-treated with ABT-737 or zVAD-fmk. To further interrogate the mechanism of cell death engaged by each perturbagen, we replicated this treatment strategy in DKO MEFs (Figure 2C). DKO MEFs treated with VP16 demonstrated no labeling due to the requirement of BAX and BAK for mitochondrial permeabilization in the intrinsic pathway of apoptosis. However, DKO MEFs utilizing the extrinsic pathway of apoptosis or ferroptosis by TNFα and CHX co-treatment or erastin, respectively, exhibited similar kinetics of death compared to WT MEFs. Furthermore, DKO MEFs labeled were labeled by Annexin V and YOYO3 with similar kinetics. Interestingly, DKO MEFs treated with CHX alone exhibited death similar to analogously treated WT MEFs but did not synergize with ABT-737, suggesting that CHX treatment engaged multiple pathways of cell death. These data demonstrate that co-utilization of Annexin V and a viability dye such as YOYO3 reveal kinetic patterns indicative of underlying cell death biology.

Mathematical processing of SPARKL kinetic data provides several parameters for high-throughput comparative analyses.

Cell death assays using flow cytometry provide only endpoint data and are typically visualized as comparative bar graphs, quadrant plots of probe positivity, or histograms of fluorescent intensity. Kinetic data gathered from SPARKL is conducive to analyzing and comparing the time to death onset and the rate of cell death within a population in response to a perturbagen. MEFs co-treated with TNFα+CHX demonstrated sequential

labeling of Annexin V and then YOYO3, indicative of apoptotic cell death (Figure 2D). Kinetic data of the above labeling events can be directly processed to investigate the extent of this differential labeling. For example, the number of YOYO3-positive events at each time point can be subtracted from the number of Annexin V-positive events to articulate the time lag between single-positive and dual-positive labeling (Figure 2E). Positive events detected at successive time points can be expressed as a percentage of maximum population signal, and compared similarly (Figure 2F). Representation of data in this manner clearly identifies the period when differential labeling is most observed and how this period is variable between treatments. Additionally, kinetics of population cell death can be analyzed as the number of events occurring within each time interval. Histograms of events per hour reveal more rapid and robust labeling with Annexin V compared to YOYO3 in MEFs dying by apoptosis, but histograms overlap in MEFs dying by ferroptosis (Figure 2G). These data better illustrate labeling trends within the cell population and therefore can be analyzed for population statistics (such as reporting mean, median, and deviation of cell events within the population). Collectively, these analyses of SPARKL kinetic data afford investigators to directly compare rates of Annexin V and YOYO3 labeling in response to a cohort of perturbagens.

It is important to note that the kinetic data collected by SPARKL represents populations of dying cells labeling with fluorescent probes. For an individual cell, detection of fluorescent labeling is a binary process and pixels are considered “positive” when they exhibit fluorescence above a threshold value established during algorithm training. Therefore, the kinetic data of cell populations denotes parameters such as time to first or last event, time at which half the population is labeled, and time period in which most cells

within the population label. SPARKL captures images of the same cells over time and provides the opportunity for investigators to track individual event progression on a single-cell level. To demonstrate this feature, we utilized the image stacks and analysis masks generated during the SPARKL workflow and processed them using ImageJ and Fiji (Schneider et al., 2012, Schindelin et al., 2012). Fluorescent events were spatially and temporally defined as regions of interest (ROIs) and then cross-referenced between images slices and fluorescent channels. This analysis permits investigators to identify the time-to-signal for both fluorophores at any given ROI. WT MEFs were instigated to die and analyzed by this method to investigate the labeling kinetics single-cell resolution (Figure 2H). When ordered by time-to-signal-1 (Annexin V-FITC in this instance), individual cells within the population exhibited treatment-specific distributions in time-to-signal. Interestingly, the progression of cells to signal-2-positivity (YOYO3 in this instance) is highly variable, but exhibits a similar distribution within each signal-1-positive subset. At this single cell resolution, cells undergoing apoptotic cell death demonstrate consistent sequential labeling, the duration of which appears to be perturbagen- and pathway-dependent. ROIs demonstrating simultaneous co-labeling (represented by the absence of a red phase) appeared substantially more frequently in erastin-treated MEFs and instances of sequential labeling occurred much more rapidly, which is indicative of the labeling profile of cells undergoing ferroptosis. These analyses exemplify the ability of SPARKL to analyze cell death at both population- and single-cell level resolutions.

To take full advantage of the high-throughput capacity of SPARKL, key parameters within the collected data need to be identified and quantified for comparative analyses. Here, we will demonstrate several methods for mathematically processing data collected

from SPARKL and extracting parameters for treatment comparisons (Figure 3A). The curves of kinetic labeling can be visually simplified into a single parameter without loss of depth by calculating the area under the curve (AUC). WT and DKO MEFs were instigated to die using a variety of perturbagens, co-treated with ABT-737 or zVAD-fmk, and detected by Annexin V- and YOYO3-labling (Figure 3B). AUC values were greater in cells co-treated with ABT-737 and reduced in cells co-treated with zVAD-fmk for perturbagens activating apoptosis, but unchanged in cells undergoing ferroptosis. AUC calculated from YOYO3 detection exhibit similar trends in response to ABT-737 and zVAD-fmk but to a lesser degree (Figure 3B). These analyses retained the observed trends of Annexin V and YOYO3 labeling within the raw kinetic data. Another parameter of interest is the rate of cell death and the time to maximal rate of death. The first derivative was calculated for data collected from MEFs treated with pro-death perturbagens and labeled with Annexin V (Figure 3C). The derivative reports the rate of cell death within the population at each collected time point. MEFs undergoing apoptosis demonstrated greater rates of cell death at earlier time points in response to ABT-737 while exhibiting lower rates in response to zVAD-fmk (Figure 3C, yellow and purple data). Additionally, data can be presented as the time-to-maximal rate of death, however this parameter is only informative for samples exhibiting significant death and labeling by the fluorescent probes (Figure 3D). These mathematical analyses represent simple methods to parameterize data collected with SPARKL for convenient comparisons between experimental conditions.

In an effort to quantify data in a manner that better retains the richness of kinetic data, we employed a non-linear fit analysis to the data collected with SPARKL. A Lag One-Phase Exponential (LOPE) function provided the best fit for our data and has been

utilized successfully by other groups modeling cell death kinetics (Figure 3E) (Forcina et al., 2017). This mathematical function reflects the lag period prior to the onset of cell death in which cells undergo biological signal transduction in response to perturbagens. The LOPE function calculates two specific parameters during the fit analysis: the duration of the lag phase (*t'*) and the rate of cell death following the lag phase (R_D). It is worth noting that this model assumes that R_D is the maximal rate of cell death which may not always be accurate. However, this model consistently performed better when fitting data compared to other models (for example, sigmoidal functions). Plateau amplitude is dependent on the number of cells in the well and therefore was not considered for parameterization in comparative studies. Comparing t' values for WT MEFs labeled with Annexin V and undergoing apoptosis demonstrates a clear trend in which ABT-737 co-treatment reduces *t'*, while the *t'* of MEFs undergoing ferroptosis was unchanged (Figure 3F). R_D trends calculated from Annexin V data were harder to interpret since the metric only differed in MEFs co-treated with CHX and ABT-737 (Figure 3G). We believe this may be an indication that the selected perturbagen concentrations are excessive and therefore R_D has plateaued, or an indication that the time of maximal death significantly differs from the R_D calculated using LOPE. Interestingly, *t'* from YOYO3 data did not reflect changes in response to ABT-737 and R_D values increased (Figures 3F-G, red data). Viewing these data as two-parameter plots reveals treatment- or cell type-specific trends in *t'* and R_D following co-treatment with ABT-737 (Figure 3H). This strategy for data visualization has an additional advantage when characterizing mechanisms of cell death mechanisms for perturbagens of unknown biology (Forcina et al., 2017). These methods to mathematically

process data collected with SPARKL demonstrate the versatility, range of applications, and analyses investigators can apply to experimental paradigms.

Simultaneous collection of proliferation and cell death data to accurately characterize perturbagen lethality.

The high-throughput capacity of SPARKL permits investigators to conduct exhaustive optimizations and drug titrations with relative ease. However, perturbagens at sub-lethal concentrations may still affect rates of cell proliferation, either directly or as a consequence while mitigating the stress signal. Therefore, investigators require a method to properly assess the cytostatic effects of perturbagens on cells in culture. This is commonly accomplished by either measuring confluency or surface area metrics, which do not accurately reflect cell numbers, or by requiring the investigator to generate cell lines stably expressing fluorescent proteins, which is laborious, limiting to model systems, and not conducive to high-throughput analyses (Artymovich and Appledorn, 2015). Previously, we described a method utilizing non-toxic CFSE to label cells prior to treatment and data acquisition (Gelles and Chipuk, 2016). This method required additional handling steps, suffered mild photobleaching, and was not compatible with certain cell types. Therefore, we sought to develop a label-and-go protocol of SPARKL that would simultaneously collect proliferation and cell death data in real-time without requiring a separate cell-labeling step (Figure 4A).

Probes labeling the nucleus provide robust and readily detectable fluorescent events, which can be efficiently analyzed for accurate quantification of event number within each sample. However, most nuclear labeling probes are either cell impermeable

or function as toxic DNA intercalators which are incompatible with time-course experiments and the SPARKL workflow. Therefore, we investigated if cell-permeable, low-affinity cyanine nucleic acid stains were suitable for prolonged incubation with cells. MEFs were incubated with varying concentrations of SYTO fluorescent dyes and Annexin V conjugated with AlexaFluor 594 (Annexin V-594) in order to assess the cytotoxic effects of nucleotide labeling (Figure 4B). All tested SYTO dyes exhibited toxicity at high concentrations and degrees of cytostatic behavior at low- to mid-range concentrations. Low-concentration ranges of SYTO16 and SYTO21 demonstrated no adverse effects to cell proliferation or viability, and we ultimately selected SYTO21 for use within SPARKL workflows. SYTO21 primarily labeled cells in the nucleus, was readily detected and segmented by the SPARKL algorithm, and capable of labeling daughter cells post-mitosis (Figure 4C). Additionally, SYTO21 signal was retained in cells undergoing apoptosis and resulted in SYTO21/Annexin V-594 double-positive events. MEFs incubated with SYTO21 demonstrated an increase in SYTO21-positive events over time, indicative of proliferation. By contrast, MEFs undergoing apoptosis via treatment of TNFα+CHX exhibit no change in the number of SYTO21-positive events and robustly labelled with Annexin V-594 (Figure 4D). Therefore, SYTO21 is suitable as a fluorescent probe to track cell proliferation and population growth.

High-content live-cell imagers detect fluorescence and express data as a number of positive events within a given area. However, this value is not normalized for total cell number and therefore more events are detected in wells containing more cells. Interpretations of data expressed in this manner may be obfuscated when cell numbers vary between samples due to either treatment-induced or cell type-specific differences in

proliferation rates. Imperfect strategies to circumvent this issue undermine the advantages of kinetic monitoring by either implementing tandem analysis via flow cytometry or normalizing to end-point data collected using DNA-intercalating dyes or potent inducers of cell death. Therefore, we investigated whether SYTO21 labeling could be used to normalize cell death data collected with SPARKL. MEFs were seeded at several densities, incubated with SYTO21 and Annexin V-594, and treated with either vehicle or TNFα+CHX. SYTO21 data accurately measured differences in cell number and tracked cell proliferation in untreated MEFs; MEFs instigated to die exhibited constant SYTO21 data and the concomitant Annexin V-positive data exemplified how cell number can complicate data interpretation (Figure 4E). The number of Annexin V-positive events at each timepoint was normalized by the corresponding SYTO21-positive events to express data as the percent of the population exhibiting Annexin V-positivity (Figure 4F). For comparison, Annexin V-positive endpoint data collected using SPARKL is shown both as the raw number of events and the adjusted percentages normalized using total cell number as reported by SYTO21 (Figure 4G). These data demonstrate that when coupled with skilled cell culture practices, this dual-labeling method and analysis can control for cell number differences due to differential cell seeding and cell type-inherent or treatment-induced alterations to proliferation rates.

Cell death data normalization by SYTO21-labeling is particularly relevant when perturbagens do not illicit a rapid death phenotype, which will result in more proliferation variability between experimental conditions and therefore different maximal labeling. To demonstrate this, we applied the normalization methodology to WT and DKO MEFs, which exhibit dramatic differences in rates of proliferation, incubated with SYTO21 and

Annexin V, and treated with a panel of perturbagens. Annexin V data collected through SPARKL was normalized by the SYTO21 data and provided values that can be directly compared between the two cell types (Figure 5A). Perturbagens engaging BAX- and BAK-mediated apoptosis demonstrated an attenuated lethal response in DKO MEFs (such as VP16 and calcium ionophore, A23187) and perturbagens capable of engaging the intrinsic pathway of apoptosis were synergized by co-treatment with ABT-737. When we replicated this experiment using YOYO3 as the cell death probe and normalized for SYTO21 labeled cells, we observed a significant loss of signal during longer experiments (Figure 5B). When analyzed for longer than 24 hours, MEFs undergoing apoptosis by co-treatment with TNFα+CHX exhibited sustained SYTO21- and Annexin V-positivity, but demonstrated a loss of YOYO3 signal over time (Figure 5C). We analyzed the average fluorescent intensity of positive events which revealed that YOYO3-positive events lost fluorescence over time (Figure 5D). While photobleaching may contribute to this loss of signal, we believe that the effect is indicative of changes to DNA content and subsequent labeling by YOYO3, which would explain why the diminished signal is perturbagen-specific. Signal loss does not appear to be due to cells leaving the focal plane as this would affect detection of all probes, and the data do not demonstrate this concomitant loss of signal in either SYTO21 or Annexin V over time. Therefore, we suggest coupling Annexin V with SYTO21 for long-duration analyses.

We capitalized on this method to normalized data and the same mathematical analyses described previously. Percentages of cell death calculated by normalizing Annexin V data to SYTO21 were fit using the LOPE function (Figure 5E). Samples co-treated with ABT-737 reveal a reduction in lag phase time (t'), indicative of BCL-2 family

contributions within the cell death pathway; by contrast, *t'* is unchanged in response to ABT-737 in MEFs undergoing ferroptosis via erastin (Figure 5F). Interestingly, receptor-mediated apoptosis by either TNFα or TRAIL in conjunction with CHX demonstrated substantially different kinetics when co-treated with ABT-737, which may indicate the preference for either Type I or Type II cell death pathways downstream of death receptor signaling. When comparing the initial rates of cell death (R_D), we observed increased rates in of death following co-treatment of ABT-737 in MEFs treated with CHX, TNFα+CHX, TRAIL+CHX, or VP16 (Figure 5G). R_D was unchanged in MEFs treated with erastin and also unchanged in MEFs treated with A23187. Cell death data from MEFs treated with A23187 collectively indicates a mechanism requiring BAX and BAK but only partially sensitized by inhibition of anti-apoptotic BCL-2 proteins, which is a profile not shared amongst the other perturbagens exampled within this work (Figure 5H). Control-treated MEFs demonstrated ambiguous fit curves and therefore parameter extraction was highly variable and not informative (Figures 5E-G, red panel). Similarly, DKO MEFs not exhibiting death in response to particular perturbagens (such as VP16 and A23187) produced ambiguous fit curves and were not analyzed further (data not shown). These data exemplify the utility of these analyses when fit to data normalized for differential cell numbers as a consequence of cell-inherent or treatment-induced changes to proliferation.

Discussion

Here we described the SPARKL workflow which is capable of simultaneously gathering proliferation and cell death data at single-cell and population-level resolutions. Using multiplex fluorescent detection of cell death, investigators can dichotomize cells engaging apoptotic or non-apoptotic signaling pathways in response to perturbagens. Additionally, we described a method to quantify cell numbers and proliferation using a non-disruptive fluorescent probe which is compatible with “label-and-go” workflows conducive to high-throughput studies. Collection of these rich datasets provides more comprehensive insight into the cytostatic effects of perturbagens as well as their cytotoxic potential. Furthermore, we described and expand upon robust and thorough mathematical analyses that parameterize data for convenient comparative analyses and interpretations of underlying cell death biology. The presented data demonstrate the versatility of the technology using single concentration treatments, but these workflows and analyses are well suited for experiments using perturbagen titrations and determining optimal conditions for subsequent studies. Collectively, SPARKL is a versatile, data-rich, non-intensive, and zero-handling method to visualize, detect, and quantify the kinetics of cell death which, when coupled with mathematical analyses, enable investigators to conduct thorough high-throughput comparative studies.

Limitations

The data presented herein have utilized immortalized MEFs to demonstrate the workflows compatible with SPARKL. These adherent cells demonstrate minimal PS exposure under normal growth conditions. In our method, cells are incubated with labeled Annexin V

which may bind stochastically-exposed PS on the outer leaflet of the plasma membrane and result in fluorescent puncta. These puncta are easily excluded while developing appropriate processing definitions, but may pose a difficulty for cell types demonstrating significant basal PS localization on the outer leaflet. Additionally, while MEFs tolerated the use of SYTO21 as a non-perturbing cell marker, other cell lines may demonstrate increased sensitivity to the nucleotide label. During analysis, accurate quantification of fluorescent events requires segmenting neighboring fluorescent signals without inappropriately bifurcating individual events. Therefore, cell lines that grow in colonies or exhibit a “cobble-stone” monolayer may require more stringent optimization to adequately establish segmentation between neighboring cells. Finally, MEFs demonstrated minimal detachment from the plate following cell death and therefore our count of fluorescent events remained constant over the course of our assays. However, alternative cell models may not remain adherent following cell death and a fluorescent cellular marker would be required to assess loss of signal due to cells leaving the focal plane of the imager.

References

Artymovich K., Appledorn D.M. (2015). A multiplexed method for kinetic measurements of apoptosis and proliferation using live-content imaging. Methods Mol Biol. *1219*, 35-42.

Biton S., Ashkenazi A. (2011). NEMO and RIP1 control cell fate in response to extensive DNA damage via TNF-α feedforward signaling. Cell *145*, 92-103.

Chan G.K., Kleinheinz T.L., Peterson D., Moffat J.G. (2013). A simple high-content cell cycle assay reveals frequent discrepancies between cell number and ATP and MTS proliferation assays. PLoS One *8*, e63583.

Chipuk J.E., Moldoveanu T., Llambi F., Parsons M.J., Green D.R. (2010). The BCL-2 family reunion. Mol Cell *37*, 299-310.

Devaux P. (1991). Static and dynamic lipid asymmetry in cell membranes. Biochemistry *30*, 1163–1173.

Dillon C, Weinlich R, Rodriguez D, Cripps J, Quarato G, Gurung P. (2014). RIPK1 blocks early postnatal lethality mediated by caspase-8 and RIPK3. Cell *157*,1189–1202.

Dixon S.J., Lemberg K.M., Lamprecht M.R., Skouta R., Zaitsev E.M., Gleason C.E., Patel D.N., Bauer A.J., Cantley A.M., Yang W.S., Morrison B., Stockwell B.R. (2012). Ferroptosis: an iron-dependent form of nonapoptotic cell death. Cell *149*, 1060-72.

Forcina G.C., Conlon M., Wells A., Cao J.Y., Dixon S.J. (2017). Systematic Quantification of Population Cell Death Kinetics in Mammalian Cells. Cell Syst. *4*, 600-610.

Gaudet S., Spencer, S.L., Chen W.W., Sorger P.K. (2012). Exploring the contextual sensitivity of factors that determine cell-to-cell variability in receptor-mediated apoptosis. PLoS Comput Biol *8*, e1002482.

Gelles J.D., Chipuk J.E. (2016). Robust high-throughput kinetic analysis of apoptosis with real-time high-content live-cell imaging. Cell Death Dis. *8*, e2758.

Jiang L., Tixeira R., Caruso S., Atkin-Smith G., Baxter A., Paone S., Hulett M.D., Poon I.K. (2016). Monitoring the progression of cell death and the disassembly of dying cells by flow cytometry. Nat Protoc. *4*, 655-663.

Kepp O., Galluzzi L., Lipinski M., Yuan J., Kroemer G. (2011). Cell death assays for drug discovery. Nat Rev Drug Discov *10*, 221-37.

Koopman G., Reutelingsperger C., Kuijten G., Keehnen R., Pals S., van Oers M. (1994). Annexin V for flow cytometric detection of phosphatidylserine expression on B cells undergoing apoptosis. Blood *84*, 1415–1420.

Logue S., Elgendy M., Martin S. (2009). Expression, purification and use of recombinant annexin V for the detection of apoptotic cells. Nat Protoc *4*, 1383-1395.

McStay G.P., Salvesen G.S., Green D.R. (2008). Overlapping cleavage motif selectivity of caspases: implications for analysis of apoptotic pathways. Cell Death Differ. *15*, 322-331.

Meers P., Mealy T. (1993). Calcium-dependent annexin V binding to phospholipids: stoichiometry, specificity, and the role of negative charge. Biochemistry *32*: 11711–11721.

Oltersdorf T., Elmore S., Shoemaker A., Armstrong R., Augeri D., Belli B., et al. (2005). An inhibitor of Bcl-2 family proteins induces regression of solid tumours. Nature *435*, 677-81.

Onufriev M., Yakovlev A., Lyzhin A., Stepanichev M., Khaspekov L., Gulyaeva N. (2009). A secreted caspase-3-substrate-cleaving activity at low pH belongs to cathepsin B: a study on primary brain cell cultures. Biochemistry (Mosc) *74*, 281-287.

Peltzer N., Darding M., Walczak H. (2016) Holding RIPK1 on the Ubiquitin Leash in TNFR1 Signaling. Trends Cell Biol. *26*, 445-461.

Schneider, C.A., Rasband, W.S., Eliceiri, K.W. (2012). NIH Image to ImageJ: 25 years of image analysis. Nat Methods *9*, 671-675.

Schindelin, J., Arganda-Carreras, I., Frise, E. (2012). Fiji: an open-source platform for biological-image analysis. Nat Methods *9*, 676-682.

Segawa K, Kurata S, Yanagihashi Y, Brummelkamp T, Matsuda F, Nagata S. (2014). Caspase-mediated cleavage of phospholipid flippase for apoptotic phosphatidylserine exposure. Science *344*, 1164–1168.

Spencer S.L., Gaudet S., Albeck J.G., Burke J.M., Sorger P.K. (2009). Non-genetic origins of cell-to-cell variability in TRAIL-induced apoptosis. Nature *21*, 428-32.

Thévenaz, P., Ruttimann, U.E., Unser, M. (1998). A Pyramid Approach to Subpixel Registration Based on Intensity. IEEE Trans Image Process *7*, 727-41.

Vanden Berghe T., Vanlangenakker N., Parthoens E., Deckers W., Devos M., Festjens N., Guerin C.J., Brunk U.T., Declercq W., Vandenabeele P. (2010). Necroptosis, necrosis and secondary necrosis converge on similar cellular disintegration features. Cell Death Differ. *17*, 922-30.

Wei M.C., Zong W.X., Cheng E.H., Lindsten T., Panoutsakopoulou V., Ross A.J., Roth K.A., MacGregor G.R., Thompson C.B., Korsmeyer S.J. (2001). Proapoptotic BAX and BAK: a requisite gateway to mitochondrial dysfunction and death. Science *292*, 727-30.

Yu K., Kennedy C.A., O'Neill M.M., Barton R.W., Tatake R.J. (2001). Disparate cleavage of poly-(ADP-ribose)-polymerase (PARP) and a synthetic tetrapeptide, DEVD, by apoptotic cells. Apoptosis *6*, 151-160.

Figure Legends

Figure 1. SPARKL provides data-rich kinetic analyses of cell death in real-time using live-cell imaging.

(**A**) Comparison of workflows for cell death detection assays using traditional flow cytometry methods or SPARKL live-cell imaging. SPARKL eliminates sample preparation and handling while coupling real-time detection and analysis into a simple, rapid, and less laborious protocol.

(**B**) MEFs were co-treated with CHX (50 µg/ml) and mTNFα (10 ng/ml) to induce cell death, incubated with titrations of Annexin V-FITC (67, 100, 133, 200, 400, 1000, 2000, and 4000 ng/ml) and YOYO3 (200, 250, 333, 400, 500, 667, 1000, and 2000 nM), and subjected to the SPARKL protocol.

(**C**) MEFs cultured in DMEM lacking or containing phenol red were treated as in ***B***. Positive labeling events were analyzed for signal intensity as mean fluorescence intensity integrated over the event area. Relative fluorescence intensity is depicted as a heat map for each titration of Annexin V-FITC and YOYO3.

(**D**) *Bak*$^{+/+}$*Bax*$^{+/+}$ (WT) and *Bak*$^{-/-}$*Bax*$^{-/-}$ (DKO) MEFs were treated with DMSO (0.2%), mTNFα (10 ng/ml) + CHX (50 µg/ml), VP16 (25 µM), or Erastin (10 µM), and incubated with Annexin V-FITC (1 µg/ml) and YOYO3 (250 nM). Images were collected by an IncuCyte ZOOM with a 10× objective and the shown panels are representative images from the stack; 100 µm scale bar. Images were white-point corrected to normalize visualization of green and red pixel background in images lacking a significant fluorescent signal.

(**E**) Kinetic data analyzed from images stacks corresponding to cells from ***D***. Dissimilar range of axis reflects differences in number of total cells due to rates of proliferation. Axis range is determined by internal controls within each experiment.

(**F**) Comparative endpoint data extracted from ***E*** at the indicated time-points.

Figure 2. Dual-reporter SPARKL protocol for interrogating mechanisms of cell death.

(**A**) Cells dying by apoptotic or non-apoptotic mechanisms exhibit differential labeling of Annexin V or a cell viability dye (YOYO3) which are not clearly differentiated by flow cytometric methodologies.

(**B**) WT MEFs were incubated in growth media containing Annexin V-FITC (1 μg/ml) and YOYO3 (250 nM), treated with CHX (50 μg/ml), mTNFα (10ng/ml) + CHX (50 μg/ml), VP16 (25 μM), or Erastin (10 μM), co-treated with DMSO, ABT-737 (1 μM), or zVAD-fmk (100 μM), and subjected to SPARKL.

(**C**) DKO MEFs were treated and incubated as in ***B***.

(**D**) Number of YOYO3-positive events was subtracted from the number of Annexin V-positive events for cells analyzed in ***B***.

(**E**) Annexin V and YOYO3 kinetic data from ***B*** expressed as the percent of maximum observed events over the duration of the experiment.

(**F**) Data calculated as in ***D*** but using the percent of maximum number of events shown in ***E***.

(**G**) Histogram data from cells treated and analyzed as in ***B*** shown as number of new events during each time interval.

(**H**) Individual cells from ***B*** were monitored and analyzed to investigate the kinetics of single- and dual-labeling following the indicated treatment.

Error bars are not shown for kinetic data to aid in data visualization.

Figure 3. Mathematical analysis of the SPARKL kinetic data provides several parameters for high-throughput comparative assays.

(**A**) Example methods for mathematically analyzing kinetic data and extracting parameters for cell death comparative studies. Area under the curve (AUC) provides a single parameter for comparing kinetic data between treatments or cell types. Mathematical conversion of kinetic data can provide additional comparative parameters such as death rates via derivatization or death onset from non-linear fit analyses.

(**B**) WT and DKO MEFs were incubated in DMEM containing Annexin V-FITC (1 μg/ml) and YOYO3 (250 nM), treated with CHX (50 μg/ml), mTNFα (10ng/ml) + CHX (50 μg/ml), VP16 (25 μM), or Erastin (10 μM), co-treated with DMSO, ABT-737 (1 μM), or zVAD-fmk (100 μM), and subjected to SPARKL. Area under the curve (AUC) values were calculated from kinetics of Annexin V- and YOYO3-labeling. Dissimilar range of axis reflects differences in number of total cells due to rates of proliferation. Axis range is determined by internal controls within each experiment.

(**C**) First derivative of data collected from cells treated as in ***B*** depicting the rates of population cell death at each time point.

(**D**) Comparison of maximum rates of death as calculated from first derivatives in ***C***.

(**E**) Fit curves using a Lag One-Phase Growth function (solid line) applied to data from cells treated in ***B*** (dotted line). Curve for YOYO3 labeling kinetics in cells treated with

VP16 and zVAD-fmk was considered an ambiguous fit and therefore excluded from parameter extraction and comparisons.

(**F**) Comparison of lag phase time (t') from Annexin V and YOYO3 data fits for cells treated as indicated from ***E***.

(**G**) Comparison of initial/maximal rate of death (R_D) from Annexin V and YOYO3 data fits for cells treated as indicated from ***E***.

(**H**) 2D graphs of parameters calculated in ***E*** and graphed in ***F*** and ***G*** provide a convenient method for comparing treatment trends across labels and cell types.

Error bars are not shown in instances where they are smaller than the data symbol.

Figure 4. Non-toxic label-and-go reagents used with SPARKL can normalize data to account for changes in cell proliferation.

(**A**) Label-and-go method to collect proliferation data during Annexin V-binding assay for composite cytostatic and cytotoxic effects of perturbagens.

(**B**) WT MEFs were incubated with titrations of SYTO nucleotide labeling reagents (0.03-20 μM) in the presence of Annexin V-594 (1 μg/ml) and subjected to SPARKL in order to assess toxicity of the SYTO dyes.

(**C**) WT MEFs were co-treated with CHX (50 μg/ml) and mTNFα (10 ng/ml) and incubated with Annexin V-594 (1 μg/ml) and SYTO21 (300 nM). Images captured at indicated time-points.

(**D**) Kinetic data analyzed from images stacks corresponding to cells from ***C***.

(**E**) WT MEFs were seeded at the indicated numbers 24 hours prior to treatment with mTNFα (10 ng/ml) + CHX (50 μg/ml) and incubation with Annexin V-594 (1 μg/ml) and

SYTO21 (300 nM). Cells were then subjected to SPARKL to analyze proliferation and cell death kinetics.

(**F**) Cell death data from ***E*** was normalized using SYTO21 and expressed as percentage of the population exhibiting death (% Death).

(**G**) Endpoint data of Annexin V-594-positive events from ***E*** and corresponding percent death (% Death) normalization from ***F***.

Figure 5. Parameters extracted from non-linear fit analyses of normalized death kinetics generate comparative profiles for studying mechanisms of cell death.

(**A**) WT and DKO MEFs were incubated in DMEM containing SYTO21 (300 nM), Annexin V-549 (1 µg/ml), indicated treatments of CHX (50 µg/ml), TRAIL (25 ng/ml) + CHX (50 µg/ml), mTNFα (10 ng/ml) + CHX (50 µg/ml), VP16 (25 µM), Erastin (10 µM), or A23187 (5 µM), co-treated with either DMSO control or ABT-737 (1 µM), and subjected to SPARKL workflow. Percent death (% Death) was calculated by Annexin V data normalized by the SYTO21 data at each timepoint.

(**B**) Cells, treatments, and analysis as in ***A*** for cells cultured in DMEM containing SYTO21 (300 nM) and YOYO3 (250 nM).

(**C**) WT MEFs treated as in ***A*** were subjected to long-term, repetitive detection of SYTO21-, Annexin V-594-, and YOYO3-positive events to assess signal permanence and longevity.

(**D**) Average integrated intensity of events detected in ***C*** showing photobleaching of fluorescent reporters over the first 48 hours.

(**E**) Fit curves using a Lag One-Phase Growth function applied to data from WT cells in ***A***. Curve for DMSO-treated cells was considered an ambiguous fit and therefore its parameterization is variable.

(**F**) Comparison of lag phase time (t') from fits applied to cells treated as indicated in ***A***.

(**G**) Comparison of initial/maximal rate of death (R_D) from fits applied to cells treated as indicated in ***A***.

(**H**) 2D graph of parameters calculated in ***E*** and graphed in ***F*** and ***G*** provides a convenient method for comparing trends across various cytotoxic treatments. Error bars are not shown for kinetic data to aid in data visualization, and not shown in instances where they are smaller than the data symbol.

Materials and Methods

Reagents and equipment

Cell culture reagents and chemicals were from Sigma Aldrich (St. Louis, MO, USA) or Thermo Fisher Scientific (Waltham, MA, USA) unless otherwise stated. Drugs and biologics as follows: ABT-737 (Abbott Pharmaceuticals, Lake Bluff, IL, USA); CHX (Sigma); YOYO3 and SYTO reagents (Life Technologies/Thermo Fisher Scientific), mTNFα and mTRAIL (Peprotech, Rocky Hill, NJ, USA); zVAD-fmk (ApexBio, Houston, TX, USA). Recombinant Annexin V was purified, labelled with FITC or Alexa Fluor 594 (Thermo Fisher Scientific), and re-purified using Dye Removal Columns (Thermo Fisher Scientific) following conjugation. Purity, stability, and fluorescence of labelled recombinant Annexin V was verified by SDS-PAGE and Flow Cytometry as previously described (Logue et al., 2009).

Cell culture and treatments

Experiments were performed with *Bak*$^{+/+}$*Bax*$^{+/+}$ and *Bak*$^{-/-}$*Bax*$^{-/-}$ (WT and DKO, respectively) SV40-transformed MEFs (ATCC, Manassas, VA, USA). Cells were cultured in DMEM containing 10% FBS, 2 mM L-glutamine and antibiotics and maintained in humidified incubators at 37˚C with 5% CO_2. For kinetic studies, cells were seeded at approximately 2 – 4 × 10^3 cells/well in a 96-well format and left to adhere for 24 hours. Prior to live-cell imaging, growth media was replaced with complete phenol-red-free DMEM containing indicated fluorescent reagents and perturbagens. DMEM contains sufficient calcium concentrations for robust Annexin V labeling but other media formulations require calcium supplementation for optimal Annexin V labeling (1.5 – 2 mM

716 $CaCl_2$). Plates were pre-warmed prior to data acquisition to avoid condensation and
717 expansion of the plate, which hinders auto-focusing during scan intervals. All tissue
718 cultures were confirmed mycoplasma free with the colorimetric PlasmoTest detection kit
719 (Invivogen, San Diego, CA, USA).
720
721 **SPARKL data acquisition and automated analysis**
722 Kinetic experiments were performed with the IncuCyte ZOOM (Model 4459, Essen
723 Bioscience, Ann Arbor, MI, USA) residing in a tissue culture incubator maintained as
724 above, but other high-content live-cell fluorescent imagers are capable of replicating
725 these data (e.g., IN CELL analyzer). Experiments were conducted for 24 – 96 hours with
726 data collection every 1 – 2 hours to avoid photobleaching of fluorescent reporters. Using
727 the 10× objective, a single plane of view was collected per well for 96-well plate assays.
728 Phase contrast, green channel (Ex: 440/80 nm; Em: 504/44 nm; acquisition time: 400 ms),
729 and red channel (Ex: 565/05 nm; Em: 625/05 nm; acquisition time: 800 ms) were collected
730 for all experiments with spectral unmixing set as 3% of red removed from green. Images
731 collected were 1392 × 1040 pixels at 1.22 μm/pixel. Automated image analysis was
732 accomplished using the ZOOM software (V2018A) and defined by images collected using
733 the specific cell lines and fluorescent reporters pertaining to the experiment. Processing
734 definitions were designed using the settings for each fluorescent reporter as described
735 below (Table 1). Data were always expressed as events per well. Fluorescent intensity
736 data were analyzed using the average integrated intensity (AU × μm^2) metric. Images of
737 cell culture presented in this manuscript were white-point corrected for clarity and
738 normalization of automated background subtraction in the green and red channel when

no significant fluorescent event was detected. White-point correction was accomplished by adjusting temperature and tint channels to overlap peak contributions of red, green, and blue pixels.

Table 1: Channel settings for each fluorescent reporter used for processing definitions with the IncuCyte ZOOM

	Channel	*Parameters*	*Radius (μm)*	*Threshold (RFU)*	*Edge Sensitivity*	*Area (μm^2)*
Annexin V-AF594	Red	Top-Hat	10	5	-35	>150
Annexin V-FITC	Green	Top-Hat	25	3	-30	>100
Annexin V-FITC (low)	Green	Top-Hat	25	2	-30	>50
SYTO21	Green	Top-Hat	25	0.5	-25	>150
YOYO3	Red	Top-Hat	10	3	-46	>150

Parameter extraction, mathematical processing, and data handling

Data exported from the IncuCyte ZOOM software was organized, handled, and analyzed using Excel v16.16.1 (Microsoft) and Prism 7.0d (Graphpad Software Inc.). Axis range for graphs was determined by internal negative and positive controls within each experiment. Event count data were converted into histograms using Equation 1, where #Signal$^+$ refers to the number of events using either fluorescently-labeled Annexin V or YOYO3 for a given well "*i*" at time point "*j*":

$$\#\text{Events/hour}_{\text{well=i,time=j}} = \left(\#\text{Signal+}_{i,j} - \#\text{Signal+}_{i,j-1}\right) \quad \text{(Equation 1)}$$

Area under the curve (AUC) values were calculated with the analysis tool in Prism and utilized the trapezoid rule ignoring peaks that were less than 10% of the distance from minimum to maximum Y values. The first derivative of collected data was calculated with the analysis tool in Prism and smoothed the data using 4 neighbors and 2nd order

smoothing polynomial. Non-linear curve fits were calculated using the plateau followed by one-phase association function in Prism using the least squares fitting method given by Equation 2. Parameters extracted by Equation 2 are defined as follows: *D(t'')* is the amount of death for given time point *t''*; D_0 is the initial and minimum amount of death; D_M is the plateau of maximal death; R_D is the initial and maximal rate of death; *t'* is the time at which the lag plateau ends and exponential increase in death begins. All parameters were left unconstrained for mathematical fitting. Fits listed as ambiguous by Prism only occurred in conditions that did not result in death positivity and are highlighted in the text.

$$D(t'') = D_0 + (D_M - D_0)\left(1 - e^{-R_D(t''-t')}\right) \qquad \text{(Equation 2)}$$

Experiments using SYTO21 to normalize data with cell counts was accomplished using Equation 3, where #Dead was determined by the event counts using either fluorescently-labeled Annexin V or YOYO3 for a given well "*i*" at time point "*j*":

$$\%\text{Death}_{\text{well}=i,\text{time}=j} = \left(\frac{\#\text{Dead}_{i,j}}{\#\text{SYTO+}_{i,j}}\right) \qquad \text{(Equation 3)}$$

Unless otherwise noted, all experiments were conducted in triplicate and the presented data are the mean of replicates and representative of repeated experiments. When shown, error bars denote standard deviation of replicates; select graphs omit error bars for convenience of visualization.

Individual cell event kinetics

For experiments investigating sequential labeling of individual cell events, analysis utilized event masks generated by the ZOOM software which were exported for further processing using external software packages. Specifically, masks corresponding to the channel detecting the first event (green channel, in this implementation) and the mask of

Green/Red double positive overlays were used; alternative strategies could analyze the green and red channels independently, but we found the overlay mask simplified analysis and increased throughput of image processing. Cell events were recognized and spatio-temporally defined using ImageJ and Fiji software packages (ImageJ, National Institutes of Health, Bethesda, ML, USA) (Schneider et al., 2012, Schindelin et al., 2012). Images exported from the ZOOM software were imported into ImageJ as stacks, converted to 8-bit grayscale and binary, and subjected to translation alignment using the StackReg and TurboReg plugins (Thévenaz et al., 1998). Reference regions of interest (ROIs) were autonomously defined by applying the Analyze Particles tool on the final image slice of the overlay mask. These reference ROIs were applied to all slices within the image stacks corresponding to the green and overlay channels using the Multi-Measure tool. Positive pixel intensity within ROIs defined the slice at which Signal 1 (green channel) and Signal 2 (overlay channel) occurred. These data were then sorted and aligned in Excel by ROI reference number, thereby linking identified signal slices from each channel to the same ROI for graphing and interpretation.

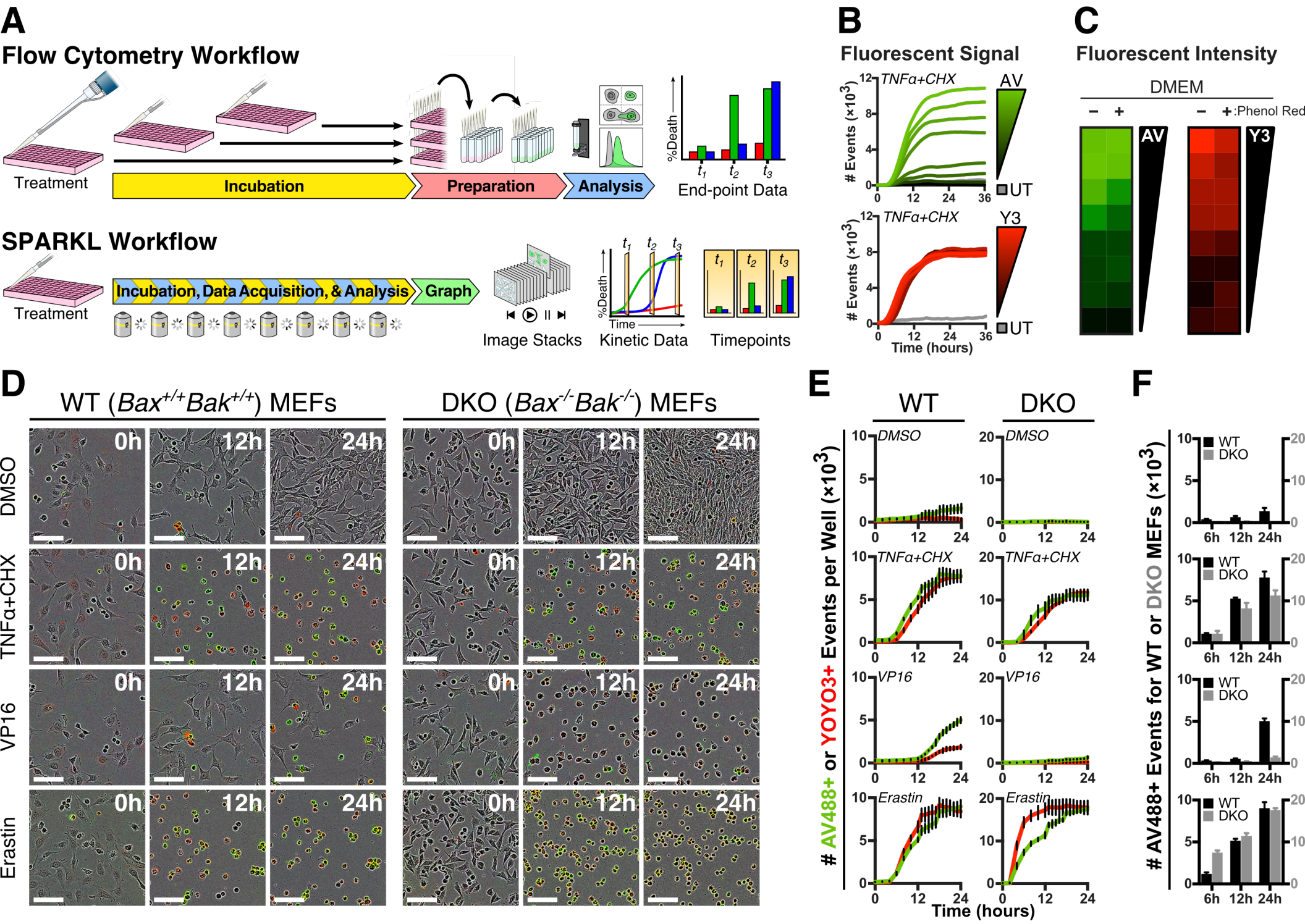
A
Flow Cytometry Workflow
Treatment
Incubation
Preparation
Analysis
%Death
End-point Data
SPARKL Workflow
Treatment
Incubation, Data Acquisition, & Analysis
Graph
Image Stacks
Kinetic Data
Timepoints
B
Fluorescent Signal
TNFα+CHX
AV
UT
Y3
Events (×10³)
Time (hours)
C
Fluorescent Intensity
DMEM
+:Phenol Red
AV
Y3
D
WT (Bax+/+Bak+/+) MEFs
DKO (Bax-/-Bak-/-) MEFs
DMSO
TNFα+CHX
VP16
Erastin
0h
12h
24h
E
WT
DKO
AV488+ or YOYO3+ Events per Well (×10³)
Time (hours)
F
AV488+ Events for WT or DKO MEFs (×10³)
WT
DKO
6h
12h
24h

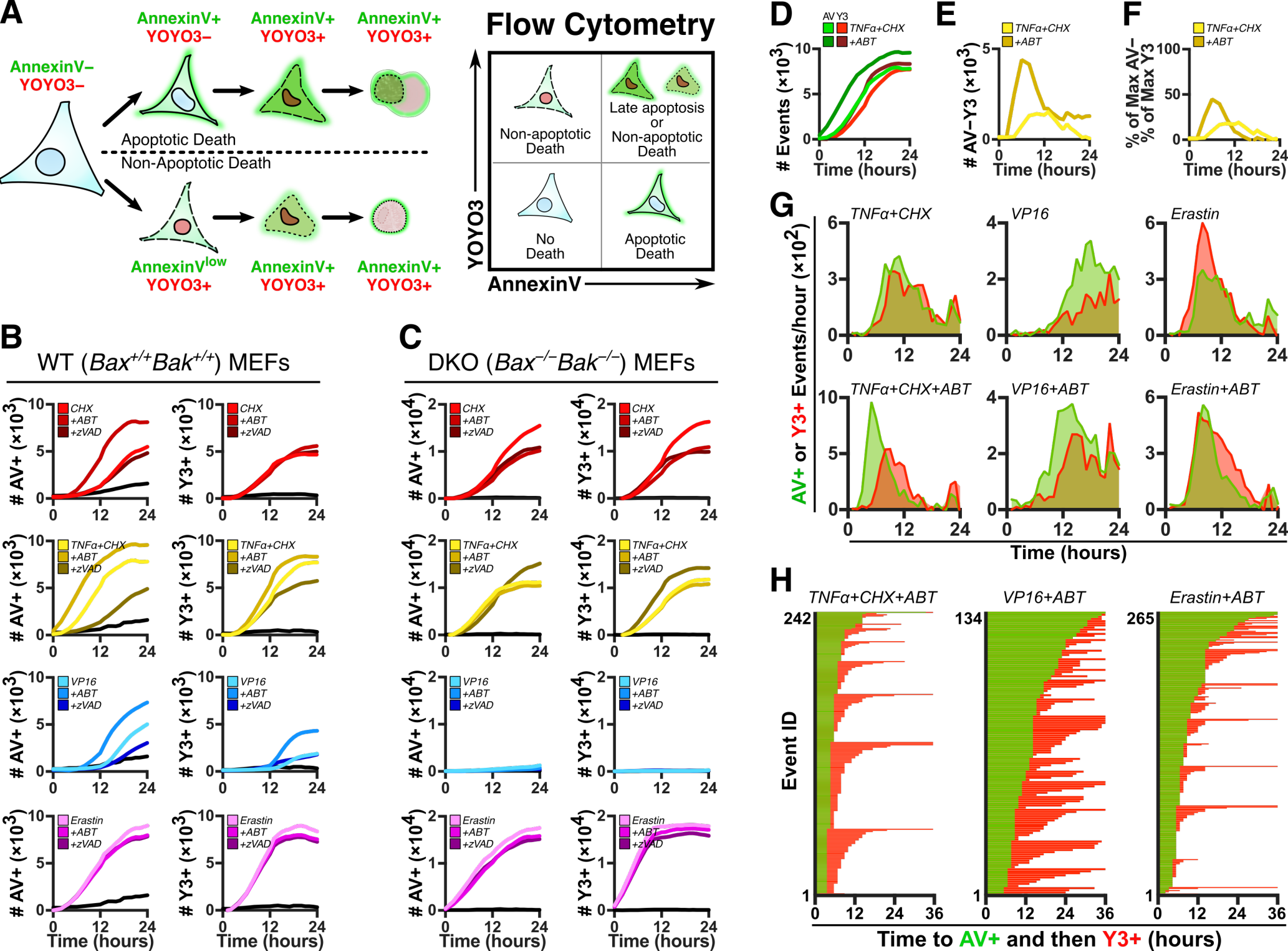
A
AnnexinV−
YOYO3−
AnnexinV+
YOYO3−
AnnexinV+
YOYO3+
AnnexinV+
YOYO3+
Apoptotic Death
Non-Apoptotic Death
AnnexinV^low
YOYO3+
AnnexinV+
YOYO3+
AnnexinV+
YOYO3+
Flow Cytometry
Non-apoptotic Death
Late apoptosis or Non-apoptotic Death
No Death
Apoptotic Death
YOYO3
AnnexinV
B
WT (Bax+/+Bak+/+) MEFs
C
DKO (Bax−/−Bak−/−) MEFs
CHX +ABT +zVAD
TNFα+CHX +ABT +zVAD
VP16 +ABT +zVAD
Erastin +ABT +zVAD
AV+ (×10^3)
Y3+ (×10^3)
AV+ (×10^4)
Y3+ (×10^4)
Time (hours)
D
AV Y3
TNFα+CHX +ABT
Events (×10^3)
Time (hours)
E
TNFα+CHX +ABT
AV−Y3 (×10^3)
Time (hours)
F
TNFα+CHX +ABT
% of Max AV− / % of Max Y3
Time (hours)
G
TNFα+CHX
VP16
Erastin
TNFα+CHX+ABT
VP16+ABT
Erastin+ABT
AV+ or Y3+ Events/hour (×10^2)
Time (hours)
H
TNFα+CHX+ABT
VP16+ABT
Erastin+ABT
242
134
265
Event ID
Time to AV+ and then Y3+ (hours)

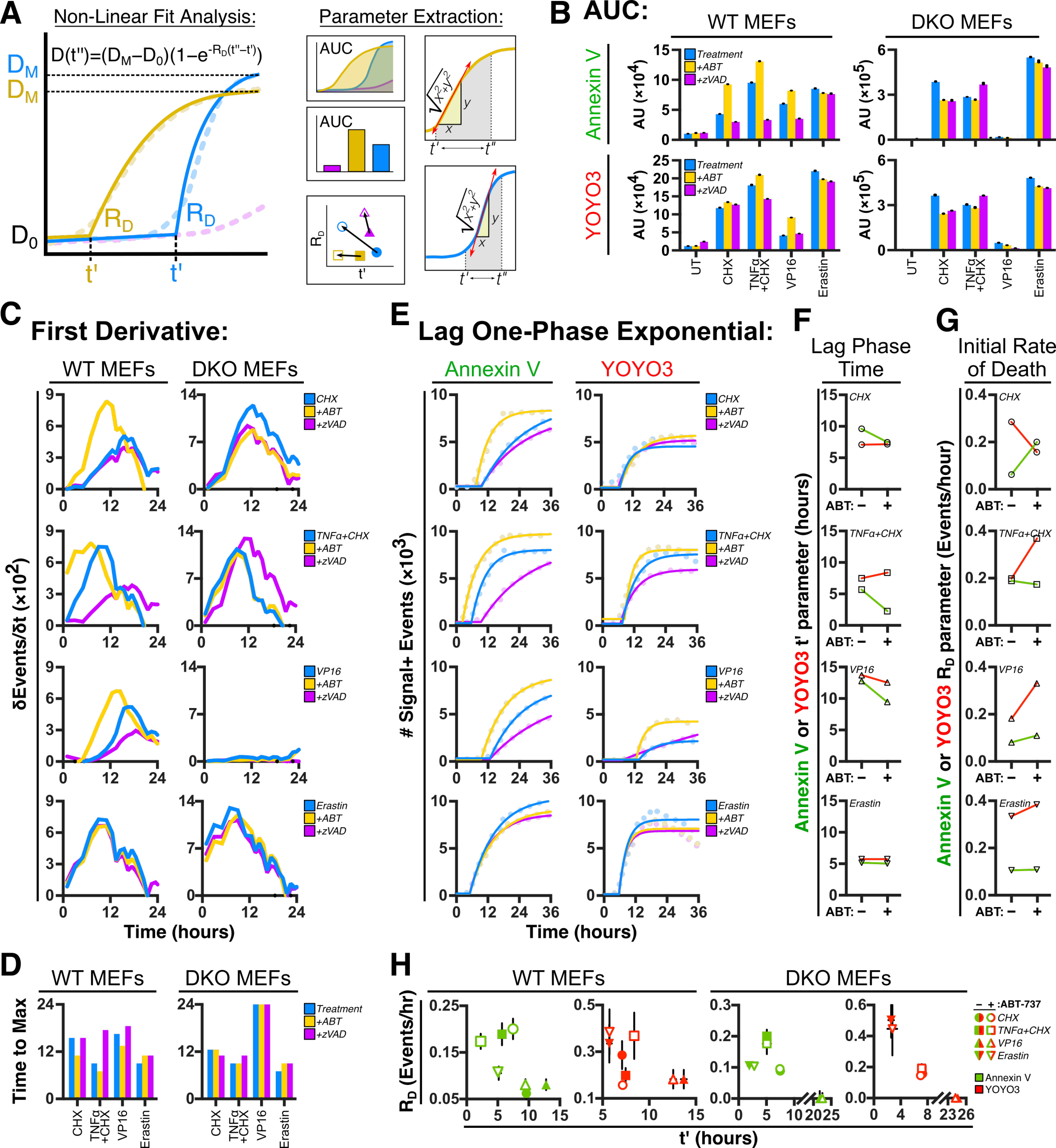
A
Non-Linear Fit Analysis:
Parameter Extraction:
D(t'')=(D_M−D_0)(1−e^{−R_D(t''−t')})
D_M
D_M
D_0
R_D
R_D
t'
t'
AUC
AUC
R_D
t'
y
x
t'
t''
B
AUC:
WT MEFs
DKO MEFs
Annexin V
YOYO3
Treatment
+ABT
+zVAD
AU (×10^4)
AU (×10^5)
UT
CHX
TNFα +CHX
VP16
Erastin
C
First Derivative:
WT MEFs
DKO MEFs
CHX
+ABT
+zVAD
TNFα+CHX
VP16
Erastin
δEvents/δt (×10^2)
Time (hours)
E
Lag One-Phase Exponential:
Annexin V
YOYO3
Signal+ Events (×10^3)
Time (hours)
F
Lag Phase Time
Annexin V or YOYO3 t' parameter (hours)
ABT: − +
G
Initial Rate of Death
Annexin V or YOYO3 R_D parameter (Events/hour)
ABT: − +
D
WT MEFs
DKO MEFs
Time to Max
Treatment
+ABT
+zVAD
CHX
TNFα +CHX
VP16
Erastin
H
WT MEFs
DKO MEFs
R_D (Events/hr)
t' (hours)
− + :ABT-737
CHX
TNFα+CHX
VP16
Erastin
Annexin V
YOYO3

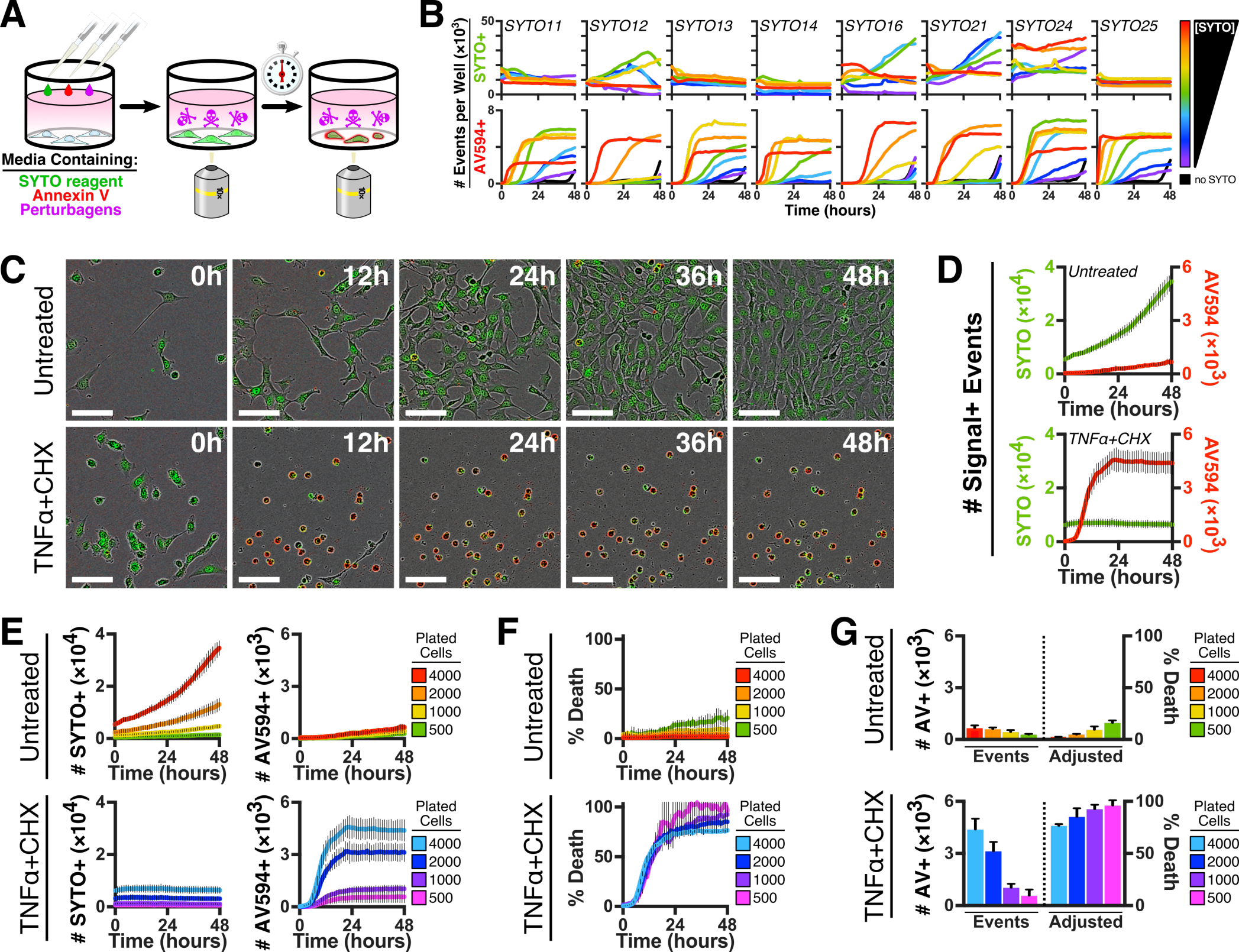
A
Media Containing:
SYTO reagent
Annexin V
Perturbagens
B
SYTO11
SYTO12
SYTO13
SYTO14
SYTO16
SYTO21
SYTO24
SYTO25
Events per Well (×10³)
SYTO+
AV594+
Time (hours)
[SYTO]
no SYTO
C
Untreated
TNFα+CHX
0h
12h
24h
36h
48h
D
Signal+ Events
Untreated
TNFα+CHX
SYTO (×10⁴)
AV594 (×10³)
Time (hours)
E
SYTO+ (×10⁴)
AV594+ (×10³)
Plated Cells
4000
2000
1000
500
F
% Death
G
AV+ (×10³)
Events
Adjusted

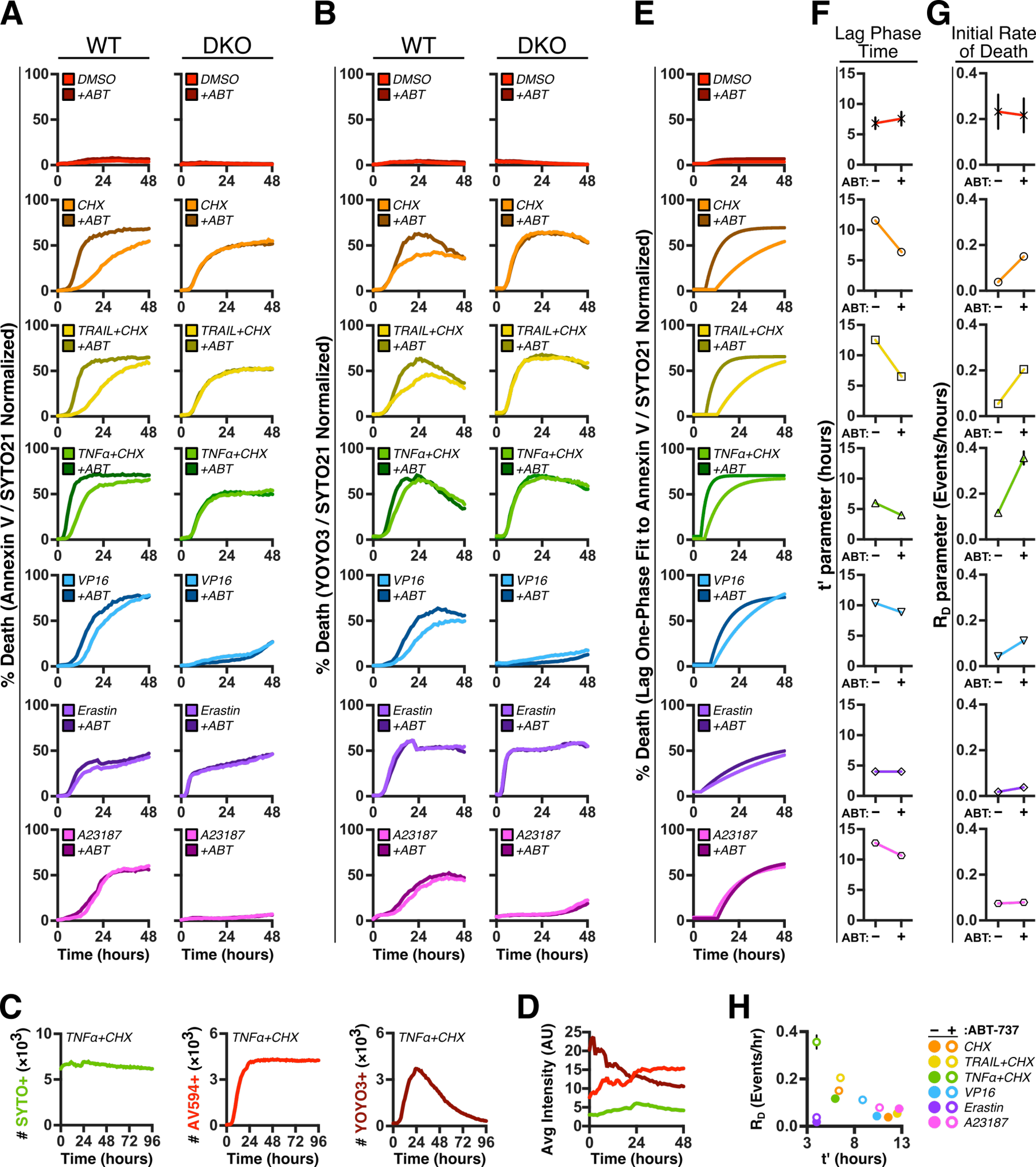
A
WT
DKO
% Death (Annexin V / SYTO21 Normalized)
DMSO
+ABT
CHX
TRAIL+CHX
TNFα+CHX
VP16
Erastin
A23187
Time (hours)
B
% Death (YOYO3 / SYTO21 Normalized)
E
% Death (Lag One-Phase Fit to Annexin V / SYTO21 Normalized)
F
Lag Phase Time
t' parameter (hours)
G
Initial Rate of Death
R_D parameter (Events/hours)
ABT: − +
C
SYTO+ (×10^3)
AV594+ (×10^3)
YOYO3+ (×10^3)
TNFα+CHX
D
Avg Intensity (AU)
H
R_D (Events/hr)
t' (hours)
− + :ABT-737
CHX
TRAIL+CHX
TNFα+CHX
VP16
Erastin
A23187